2018 European Control Conference (ECC)
June 12-15, 2018. Limassol, Cyprus

Effective angular constrained trajectory generation for thrust-propelled vehicles

Ngoc Thinh Nguyen, Ionela Prodan and Laurent Lefèvre

***Abstract*— This paper proposes a novel approach to impose constraints on angles and angular velocities for the trajectory generation of thrust-propelled underactuated vehicles. The constraints formulation requires only the translational acceleration and jerk values, without requiring the vehicle's attitude. Hence, the proposed angular constraints are satisfied even if the direction angle is designedly modified or it varies uncontrollably under unexpected events. Discussions over simulation results and comparisons with the existing methods in the literature highlight the benefits of our approach.**

***Index Terms*— Constrained trajectory generation, Thrust-propelled underactuated vehicles, Angular constraints.**

I. Introduction

Over the last few decades, research and industrial communities have shown increasing interest in thrust-propelled underactuated vehicles, e.g., tricopter, quadcopters, hexacopter, which are fast becomming a common-place in our everyday lives [1]–[5].

This paper focus is on the motion planning problem which respects the internal dynamics of such VTOL (Vertical Take-Off and Landing) systems and states and inputs constraints while optimizing certain objectives (e.g., passing through a priori given way-points, state/input constraints satisfaction, consumption minimization) [2], [6]–[8] . This is a common problem in the literature and differential flatness properties with approapiate flat output parametrizations are usually employed [9]. To take into account operating constraints within the trajectory generation problem, different constrained trajectory parametrizations are considered in the literature [4]–[7], e.g., simple monomials (elementary polynomials), Chebyshev polynomials, Laguerre polynomials [10], Bézier functions [11], B-splines functions [4], [8], etc. In particular, the angles and angular velocities constraints of the aerial systems are usually imposed based on the knowledge of a predefined yaw trajectory, e.g., zero angle [4], [10], [12] or a spline with specific degree [7]. Therefore, any change in the yaw angle trajectory (for example, designedly modified vehicle direction pointing towards the target for camera applications [7] or changes in the direction due to faulty events [3]), will obviously affect the validation of the above mentioned constraints.

In the present paper, by using flatness properties we avoid any requirements on the yaw angle values and we are still able to provide bounds for the angles and their angular velocities. Moreover, the proposed robust constraints can be used with any flat output parametrization in order to generate an optimal trajectory for the thrust-propelled system.

The remaining paper is organized as follows. Section II presents first the kinematics and dynamics modeling, then the flatness-based characterization which fully takes into account the dynamics of the thrust-propelled system. Section III details the novel approach for imposing constraints on the roll, pitch angles and the associated angular velocities. Also, detail analysis and discussions on the proposed angular constraints in combination with constraints on the thrust force are provided. Section IV presents simulation results and comparisons. Section V draws the conclusions and future work.

II. System modeling and flatness-based characterization

In this section we briefly recapitulate the kinematics and the dynamics of a standard trust-propelled underactuated vehicle (more details can be found in [1], [2]). Next, we construct the associated flatness-based characterization which allow us to perform the optimal trajectory generation subject to various constraints.

A. Kinematics

As illustrated in Fig. 1, the vehicle operates in two different coordinate systems: the *body frame* $\mathcal{B} = \{{}^{B}\boldsymbol{x}, {}^{B}\boldsymbol{y}, {}^{B}\boldsymbol{z}\}$ which is attached to the mass center and the *inertial frame* $\mathcal{I} = \{{}^{I}\boldsymbol{x}, {}^{I}\boldsymbol{y}, {}^{I}\boldsymbol{z}\}$ which is fixed to the ground. To describe the attitude of the vehicle with respect to the frame $\mathcal{I}$, we employ the roll–pitch–yaw XYZ (ϕ, θ, ψ) rotating sequence which is usually used in aerospace research [3], [11]. The associated rotation matrix is given by [1]:

$$ {}^{I}_{B}R = \begin{bmatrix} c\theta c\psi & s\phi s\theta c\psi - c\phi s\psi & c\phi s\theta c\psi + s\phi s\psi \\ c\theta s\psi & s\phi s\theta s\psi + c\phi c\psi & c\phi s\theta s\psi - s\phi c\psi \\ -s\theta & s\phi c\theta & c\phi c\theta \end{bmatrix} \quad (1) $$

Let $\Omega \triangleq \begin{bmatrix}\Omega_x & \Omega_y & \Omega_z\end{bmatrix}^\top$ be the vehicle's angular velocity in frame $\mathcal{B}$. Ω is directly related to the three Euler angles $\eta \triangleq \begin{bmatrix}\phi & \theta & \psi\end{bmatrix}^\top$ and their derivatives $\dot{\eta}$ as follows:

$$ \Omega = \begin{bmatrix} 1 & 0 & -s\theta \\ 0 & c\phi & s\phi c\theta \\ 0 & -s\phi & c\phi c\theta \end{bmatrix} \begin{bmatrix} \dot{\phi} \\ \dot{\theta} \\ \dot{\psi} \end{bmatrix} = W(\eta)\dot{\eta}. \quad (2) $$

Univ. Grenoble Alpes, Grenoble INP*, LCIS, F-26000, Valence, France.
ngoc-thinh.nguyen,ionela.prodan,laurent.lefevre@ lcis.grenoble-inp.fr.
* Institute of Engineering Univ. Grenoble Alpes.

[1]Note that, in order to write in a more compact way we have used in (1) $'c'$ and $'s'$ to denote the $\cos(\cdot)$ and $\sin(\cdot)$ functions, respectively.

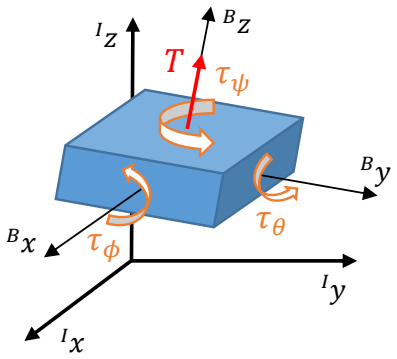

Fig. 1: Thrust-propelled vehicle and the coordinate systems.

B. Dynamics

The vehicle is considered as a rigid body with the mass m. This VTOL system is propelled by a thrust vector with magnitude T directed along the ${}^{\boldsymbol{B}}\boldsymbol{z}$ axis as illustrated in Fig. 1. Let denote by $\xi \triangleq \begin{bmatrix} x & y & z \end{bmatrix}^\top$, the position of the vehicle in frame $\mathcal{I}$. Assuming that the centrifugal force is nullified, thus, the translation dynamics are described as:

$$m\ddot{\xi} = -mg\,{}^{\boldsymbol{I}}\boldsymbol{z} + T\,{}^I_B R\,{}^{\boldsymbol{B}}\boldsymbol{z}, \tag{3}$$

where g represents the gravitational acceleration.
As presented in Fig. 1, the vehicle is equipped with some mechanism to induce torques about the three body axes [1]. Let $\tau \triangleq \begin{bmatrix} \tau_\phi & \tau_\theta & \tau_\psi \end{bmatrix}^\top$ gather the roll, pitch, yaw torques, respectively, the rotation equations are given by:

$$I\dot{\Omega} + \Omega \times I\Omega = \tau, \tag{4}$$

where $I = \mathrm{diag}\{I_{xx}, I_{yy}, I_{zz}\}$ is the symmetric inertial tensor of the vehicle in frame $\mathcal{B}$.

C. Flatness-based characterization

In the interest of optimal trajectory generation for thrust-propelled systems, a popular solution is the use of flat output characterizations [9]. Important features of flatness are well-know, as for example, it takes explicitly into account the internal dynamics of the systems and (with some difficulty) state and input constraints.

Proposition 1: The trust-propelled system defined by (2)-(4) is differentially flat with the associated flat output defined as:

$$\mathbf{z} = \begin{bmatrix} z_1 & z_2 & z_3 & z_4 \end{bmatrix}^\top = \begin{bmatrix} x & y & z & \tan\left(\frac{\psi}{2}\right) \end{bmatrix}^\top. \tag{5}$$

Proof: According to differential flatness definition [9], the necessary and sufficient conditions to assess the statement of Proposition 1 are: i) the candidate flat output $\mathbf{z}$, e.g. (5) of the general system $\dot{\mathbf{x}} = f(\mathbf{x}, \mathbf{u})$ is a function of states, inputs and their derivatives ($\mathbf{z} = \Phi(\mathbf{x}, \dot{\mathbf{x}}, \mathbf{u}, \dot{\mathbf{u}}, \dots)$); ii) the remaining states and inputs can be expressed in terms of the flat output and a finite number of its derivatives ($\mathbf{x} = \Psi_{\mathbf{x}}(\mathbf{z}, \dots, \mathbf{z}^{(q)})$, $\mathbf{u} = \Psi_{\mathbf{u}}(\mathbf{z}, \dots, \mathbf{z}^{(q+1)})$).

The first condition follows immediately from the definition of the flat output (5). The second is verified constructively. The translation dynamics (3) are explicitly expressed in terms of the flat output as:

$$m\ddot{z}_1 = T(\mathrm{c}\,\phi\,\mathrm{s}\,\theta\,\mathrm{c}\,\psi + \mathrm{s}\,\phi\,\mathrm{s}\,\psi), \tag{6a}$$
$$m\ddot{z}_2 = T(\mathrm{c}\,\phi\,\mathrm{s}\,\theta\,\mathrm{s}\,\psi - \mathrm{s}\,\phi\,\mathrm{c}\,\psi), \tag{6b}$$
$$m\ddot{z}_3 = -mg + T\,\mathrm{c}\,\phi\,\mathrm{c}\,\theta. \tag{6c}$$

Considering (6), the three Euler angles η are described as:

$$\phi = \arcsin\left(\frac{2z_4\ddot{z}_1 - (1 - z_4^2)\ddot{z}_2}{(1 + z_4^2)\sqrt{\ddot{z}_1{}^2 + \ddot{z}_2{}^2 + (\ddot{z}_3 + g)^2}}\right), \tag{7a}$$
$$\theta = \arctan\left(\frac{(1 - z_4^2)\ddot{z}_1 + 2z_4\ddot{z}_2}{(1 + z_4^2)(\ddot{z}_3 + g)}\right), \tag{7b}$$
$$\psi = 2\arctan(z_4). \tag{7c}$$

Next, the thrust T is obtained as follows:

$$T = m\sqrt{\ddot{z}_1{}^2 + \ddot{z}_2{}^2 + (\ddot{z}_3 + g)^2}. \tag{8}$$

Replacing (2) into the rotation dynamics (4) leads to the following relation of the input torques τ:

$$\tau = I\left(W(\eta)\ddot{\eta} + \dot{W}(\eta)\dot{\eta}\right) + (W(\eta)\dot{\eta}) \times (IW(\eta)\dot{\eta}). \tag{9}$$

Equations (2) and (9) indicate that the angular velocity Ω and the torque τ can be further interpreted in the flat output space by introducing (7a)–(7c) in (2) and (9), respectively, hence, completing the proof[2]. ■

III. Angular Constraints with Unspecified Yaw Angle

Considering the model with its flat representation given in Section II, this section concentrates on the generation of a feasible trajectory composed of the three position components, ξ, and the direction angle, ψ. The proposed reference trajectory has the advantage of validating the system's internal dynamics and operating constraints on the input thrust T, the roll, pitch angles ϕ, θ and their associated angular velocities Ω_x, Ω_y as defined in (2). Moreover, the trajectory will still satisfy the proposed constraints even if a predefined yaw angle is modified. In order to accomplish the trajectory generation for the thrust-propelled system, these constraints need to be employed with a specific parametrization. In our work, we prefer to use the B-splines parametrization due to its geometric and algebraic properties (i.e., convexity, ease to enforcing the continuity and the like) [8]. Note that we constrain the vehicle not to free fall, i.e., $\ddot{z} + g > 0$.

A. Constrained roll and pitch angles

This section presents a novel approach for imposing angle constraints for the trajectory generation of the thrust-propelled underactuated vehicle without any required knowledge on the yaw angle.

Proposition 2: Let us consider the trajectory generation for the thrust-propelled dynamics described in (2)–(4) with

[2]Note that the angular velocity, (2), and the torques, (9), are not explicitly written due to their convoluted representation. Nevertheless, their associated mappings are straightforward to obtain.

the flat output (5), and define the angle $\epsilon_{max} \in [0, \frac{\pi}{2})$ which verifies:

$$\max_t \left(\frac{k_1^2(t) + k_2^2(t)}{k_3^2(t)} \right) \leq \tan^2(\epsilon_{max}), \tag{10}$$

where $k_1(t) = \ddot{z}_1(t)$, $k_2(t) = \ddot{z}_2(t)$ and $k_3(t) = \ddot{z}_3(t) + g$. Then, the following inclusions:

$$\phi(t) \in [-\epsilon_{max}, \epsilon_{max}], \tag{11a}$$
$$\theta(t) \in [-\epsilon_{max}, \epsilon_{max}], \tag{11b}$$

hold regardless the yaw angle.

Proof: Recalling the flat output-derived relations (7a), (7b) and exploiting Cauchy-Schwartz inequality [13] we provide bounds for the roll and pitch angles as follows:

$$|\sin(\phi(t))| \leq \sqrt{\frac{k_1^2(t) + k_2^2(t)}{k_1^2(t) + k_2^2(t) + k_3^2(t)}}, \tag{12a}$$

$$|\tan(\theta(t))| \leq \sqrt{\frac{k_1^2(t) + k_2^2(t)}{k_3^2(t)}}, \tag{12b}$$

Further, let us define the angle $\epsilon \in \left[0, \frac{\pi}{2}\right)$ such that:

$$\tan^2(\epsilon(t)) = \frac{k_1^2(t) + k_2^2(t)}{k_3^2(t)}. \tag{13}$$

Then, after some trigonometric manipulations of (13) we obtain:

$$\sin^2(\epsilon(t)) = \frac{k_1^2(t) + k_2^2(t)}{k_1^2(t) + k_2^2(t) + k_3^2(t)}, \tag{14}$$

which allows to further express (12) as:

$$|\sin(\phi(t))| \leq |\sin(\epsilon(t))|, \tag{15a}$$
$$|\tan(\theta(t))| \leq |\tan(\epsilon(t))|. \tag{15b}$$

By introducing the constraint (10) into (13), we have that:

$$\epsilon(t) \leq \epsilon_{max}. \tag{16}$$

Lastly, (15) and (16) lead to:

$$|\sin(\phi(t))| \leq \sin(\epsilon_{max}), \tag{17a}$$
$$|\tan(\theta(t))| \leq \tan(\epsilon_{max}). \tag{17b}$$

By using the monotonic property of the $\sin(\cdot)$ and $\tan(\cdot)$ functions in the range of $\left(-\frac{\pi}{2}, \frac{\pi}{2}\right)$ in (17), we come to the conclusion that $\phi(t) \in [-\epsilon_{max}, \epsilon_{max}]$ and $\theta(t) \in [-\epsilon_{max}, \epsilon_{max}]$, hence, completing the proof. ■

Corollary 1: Combining (10) with the standard bounds for thrust (8) (see e.g., [5], [11]) which is given by:

$$T_{min} \leq m\sqrt{k_1^2(t) + k_2^2(t) + k_3^2(t)} \leq T_{max}, \tag{18}$$

it is derived that $\mathcal{K} \triangleq [k_1^2 + k_2^2 \quad k_3^2]^\top$ lies inside a polytope P defined as:

$$P = \Big\{ \mathcal{K} \in \mathbb{R}^2 : \mathcal{K} = \sum_j \alpha_j v_j, \forall \alpha_j \geq 0, \sum_j \alpha_j = 1, j = 1, \cdots, 4 \Big\}, \tag{19}$$

where the extreme points $v_j \in V, j = 1, \cdots, 4$ are parameterized after the three parameters appearing in (10), (18): ϵ_{max}, T_{min} and T_{max} as follows:

$$V = \left\{ \left(0, \frac{T_{min}^2}{m^2}\right), \left(\frac{T_{min}^2}{m^2}\sin^2\epsilon_{max}, \frac{T_{min}^2}{m^2}\cos^2\epsilon_{max}\right), \left(\frac{T_{max}^2}{m^2}\sin^2\epsilon_{max}, \frac{T_{max}^2}{m^2}\cos^2\epsilon_{max}\right), \left(0, \frac{T_{max}^2}{m^2}\right) \right\}. \tag{20}$$

Proof: With the notations from the Corollary 1, both (10) and (18) can be seen as linear inequalities involving the two non-negative terms $(k_1^2 + k_2^2)$ and k_3^2. Putting them in half-space form leads to:

$$\begin{bmatrix} 1 & -\tan^2(\epsilon_{max}) \\ -1 & -1 \\ 1 & 1 \\ -1 & 0 \\ 0 & -1 \end{bmatrix} \begin{bmatrix} k_1^2 + k_2^2 \\ k_3^2 \end{bmatrix} \leq \frac{1}{m^2} \begin{bmatrix} 0 \\ -T_{min}^2 \\ T_{max}^2 \\ 0 \\ 0 \end{bmatrix}. \tag{21}$$

Any bounded polyhedra given in half-space representation $\left(P = \{\mathcal{K} : a_i^\top \mathcal{K} \leq b_i, \forall i\}\right)$, e.g., (21) can be rewritten in generator form ($P = \{\mathcal{K} : \mathcal{K} = \sum_j \alpha_j v_j, \forall \alpha_j \geq 0, \sum_j \alpha_j = 1\}$), e.g., (19) via the Fourier-Motzkin algorithm [14]. In here, having a small number of half-spaces in $\mathbb{R}^2$, we can obtain vertices v_j in (20) by solving $a_{i'}^\top v_j = b_{i'}$, $a_{i''}^\top v_j < b_{i''}$ for all permutations of (i', i'') taken from the collection of indices $\{1, 2, 3, 4, 5\}$. E.g., v_2 is obtained by taking the 1^{st} and the 2^{nd} rows as equalities, i.e., $i' \in \{1, 2\}$ and checking that the solution holds for the three other rows of (21), i.e., $i'' \in \{3, 4, 5\}$. This utimately leads to the vertices enumerated above and thus completes the proof. ■

Illustrative example: Let us illustrate the Corollary 1 by using the VTOL dynamical system described in (2)–(4) with the parameters $m = 0.5kg$, $T_{min} = 3N$, $T_{max} = 5N$ and $\epsilon_{max} = \pi/6$. The polytope P (19) and its vertices are depicted in Fig. 2.

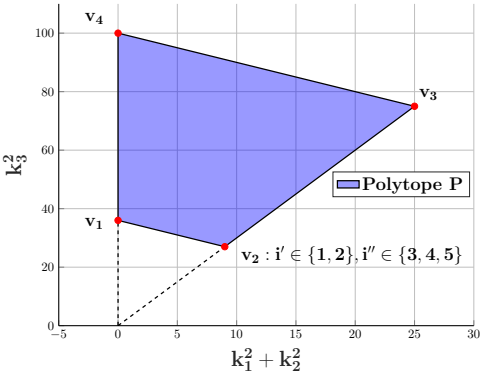

Fig. 2: Illustration of the polyhedral set P and its vertices as in (20).

B. Constrained roll and pitch angular velocities

The generation of a feasible reference trajectory requires not only angle bounds but also angular velocity bounds. In

[5], [6], the angular velocities Ω_x, Ω_y can be bounded by using the unit norm property of the rotation matrix (1). In the following, we propose a different approach to constrain the angular velocities Ω_x, Ω_y by using differential flatness which allows us to express the constraints by using only the position accelerations and the jerks.

For expressing with clarity the forthcoming results, let us define the notations:

$$\phi|_{\psi=0} \triangleq \phi_0 = \arcsin\left(\frac{-k_2}{\sqrt{k_1^2+k_2^2+k_3^2}}\right), \tag{22a}$$

$$\theta|_{\psi=0} \triangleq \theta_0 = \arctan\left(\frac{k_1}{k_3}\right), \tag{22b}$$

$$\phi|_{\psi=\pi/2} \triangleq \phi_{\pi/2} = \arcsin\left(\frac{k_1}{\sqrt{k_1^2+k_2^2+k_3^2}}\right), \tag{22c}$$

$$\theta|_{\psi=\pi/2} \triangleq \theta_{\pi/2} = \arctan\left(\frac{k_2}{k_3}\right). \tag{22d}$$

Hereinafter, we provide the bounds on the angular velocities Ω_x, Ω_y expressed in terms of the angle ϵ defined in (13) and the notations (22).

Proposition 3: Let us consider the trajectory generation for the thrust-propelled dynamics described in (2)–(4) with the flat output (5), and define the maximum operating angular velocities $\Omega_{xmax} > 0$, $\Omega_{ymax} > 0$ which verify:

$$\max_t \lambda_x(t) \leq \Omega_{xmax}, \tag{23}$$

$$\max_t \lambda_y(t) \leq \Omega_{ymax}, \tag{24}$$

where λ_x, λ_y are defined as follows:

$$\lambda_x = \frac{1}{\cos\epsilon}\sqrt{\dot{\phi}_0^2\cos^2\phi_0 + \dot{\phi}_{\pi/2}^2\cos^2\phi_{\pi/2}}, \tag{25}$$

$$\lambda_y = \sqrt{\frac{\dot{\theta}_0^2}{\cos^4\theta_0} + \frac{\dot{\theta}_{\pi/2}^2}{\cos^4\theta_{\pi/2}}}. \tag{26}$$

Then, the following inclusions:

$$\Omega_x(t) \in [-\Omega_{xmax}, \Omega_{xmax}], \tag{27a}$$

$$\Omega_y(t) \in [-\Omega_{ymax}, \Omega_{ymax}], \tag{27b}$$

hold regardless the values of the yaw angle, ψ.

Proof: As detailed in Appendix A, and with notations (22), the angular velocities Ω_x and Ω_y are expressed as:

$$\Omega_x = \frac{2z_4\dot{\phi}_{\pi/2}\cos\phi_{\pi/2} + (1-z_4^2)\dot{\phi}_0\cos\phi_0}{\cos\phi(1+z_4^2)}, \tag{28a}$$

$$\Omega_y = \frac{\cos\phi\cos^2\theta}{1+z_4^2}\left(\frac{(1-z_4^2)\dot{\theta}_0}{\cos^2\theta_0} + \frac{2z_4\dot{\theta}_{\pi/2}}{\cos^2\theta_{\pi/2}}\right). \tag{28b}$$

Using Cauchy-Schwartz inequality [13], combining it with the condition $\cos\phi \geq \cos\epsilon > 0$ (15a) for (28a) and with the conditions $\cos\phi \leq 1, \cos\theta \leq 1$ for (28b), we derive to the following inequalities:

$$|\Omega_x| \leq \lambda_x, \quad |\Omega_y| \leq \lambda_y. \tag{29}$$

Introducing (23)–(26) into (29), we obtain that the angular velocities Ω_x, Ω_y are bounded by $|\Omega_x(t)| \leq \Omega_{xmax}$ and $|\Omega_y(t)| \leq \Omega_{ymax}$, hence, completing the proof. ■

Remark 1: Note that the formulations of (25), (26) are convenient for detailing the proof of Proposition 3. However, expressing λ_x and λ_y in terms of the flat outputs z_1, z_2, z_3 and their higher derivatives, e.g., k_1, k_2, k_3 is essential for constraints implementation. Therefore, we provide in the following the explicit formulations of λ_x in (25) and λ_y in (26) which can be used for executing computer programs:

$$\lambda_x = \frac{1}{k_3}\sqrt{\left(\dot{k}_1 - k_1\kappa\right)^2 + \left(\dot{k}_2 - k_2\kappa\right)^2}, \tag{30}$$

$$\lambda_y = \frac{1}{k_3^2}\sqrt{\left(\dot{k}_1k_3 - \dot{k}_3k_1\right)^2 + \left(\dot{k}_2k_3 - \dot{k}_3k_2\right)^2}, \tag{31}$$

where $\kappa = (k_1\dot{k}_1 + k_2\dot{k}_2 + k_3\dot{k}_3)/(k_1^2+k_2^2+k_3^2)$.

Remark 2: Note also that the proposed formulations (30), (31) are different from the angle rate boundaries detailed in [5], [6]. In [5], it is stated that $|\Omega_{x,y}| \leq \Omega_b$ and in [6], $|\Omega_{x,y}| \leq \Omega_b'$, where Ω_b and Ω_b' are formulated with the above notations as:

$$\Omega_b = 2\sqrt{\frac{\dot{k}_1^2+\dot{k}_2^2+\dot{k}_3^2}{k_1^2+k_2^2+k_3^2}}, \quad \Omega_b' = \frac{\Omega_b}{2}. \tag{32}$$

We indicate that our proposed constraints are tighter than both Ω_b and Ω_b' as will be illustrated in the simulation results.

Finally, this section proposed original approaches for imposing constraints on the input thrust T (18), the roll, pitch angles (10) and their associated velocities (23), (24) within the trajectory generation of thrust propelled dynamics. The constraints have been ultimately expressed involving the position accelerations $\ddot{\xi}$ and the jerks $\xi^{(3)}$. Even with a new yaw trajectory, as long as employing the resulted reference positions ξ, the proposed constraints are validated for the associated references. These results are highlighted in the forthcoming simulations and comparison.

IV. Simulation results

The thrust-propelled underactuated system given in (2)-(4) is characterized by the following parameters:

- $m = 0.5kg$, $I_{xx} = I_{yy} = 5.2\times10^{-3}kgm^2$, $I_{zz} = 8\times10^{-3}kgm^2$.

B-spline basis functions of degree 5 are considerd for the flat output parametrization. An optimization problem which minimize the total trajectory length as in [8], [15] is implemented. As presented in Table I, the constraints include passing through three a priori given way-points $\left\{\begin{bmatrix}0 & 0 & 0\end{bmatrix}^\top, \begin{bmatrix}1.5 & 3 & 1\end{bmatrix}^\top, \begin{bmatrix}1 & 2 & 0\end{bmatrix}^\top\right\}$ with the associated time instants $\{0, 5, 10\}$ sec, respecting all the derivatives of $\{x, y, z\}$ up to 3^{th} order equal 0 at the initial and final time instants. Furthermore, the roll and pitch angles are constrained to lie inside $[-6, 6]^\circ$ by employing (10) with $\epsilon_{max} = 6^\circ$. The thrust T is also bounded by $T_{min} = 4.8N$ and $T_{max} = 5.1N$ by using (18) as introduced in Corollary 1. Moreover, the angular velocities Ω_x, Ω_y have

to stay inside the safety region defined by $[-8, 8]^\circ/sec$. These constraints are implemented by employing (23), (24) with $\Omega_{xmax} = \Omega_{ymax} = 8^\circ/sec$. The optimal trajectory generation algorithms are implemented by using Yalmip [16] in Matlab 2015a which provides us the processing time of 102 sec.

TABLE I: Constraints imposed on the optimal trajectory generation

	Constraints
Position, ξ	$\xi(0) = [0 \quad 0 \quad 0]^\top$, $\xi(5) = [1.5 \quad 3 \quad 1]^\top$, $\xi(10) = [1 \quad 2 \quad 0]^\top$
Velocity, $\dot{\xi}$	$\dot{\xi}(0) = [0 \quad 0 \quad 0]^\top$, $\dot{\xi}(10) = [0 \quad 0 \quad 0]^\top$
Acceleration, $\ddot{\xi}$	$\ddot{\xi}(0) = [0 \quad 0 \quad 0]^\top$, $\ddot{\xi}(10) = [0 \quad 0 \quad 0]^\top$
Jerk, $\xi^{(3)}$	$\xi^{(3)}(0) = [0 \quad 0 \quad 0]^\top$, $\xi^{(3)}(10) = [0 \quad 0 \quad 0]^\top$
Angles, ϕ, θ	$\phi \in [-6, \ 6]^\circ$, $\theta \in [-6, \ 6]^\circ$
Yaw angle, ψ	$\psi_1(t) = 0$, $\psi_2(t) = 2t \ \forall t \in [0, 10]$
Ω_x, Ω_y	$\Omega_x \in [-8, \ 8]^\circ/sec$, $\Omega_y \in [-8, \ 8]^\circ/sec$
Thrust, T	$T_{min} = 4.8N$, $T_{max} = 5.1N$

We provide illustrations of simulation results for two scenarios:

Scenario 1: The prior yaw reference, ψ_1 is imposed to be zero, $\psi_1(t) = 0$, along the simulation horizon. Thus, the optimal trajectory is defined by $\{x, y, z, \psi_1\}$ subject to the constraints described above;

Scenario 2: The yaw reference, ψ_2, is increasing steadily from 0 rad to 20 rad in 10 sec. Next, we employ the prior position references $\{x, y, z\}$ and ψ_2 to calculate the references of the other states and inputs.

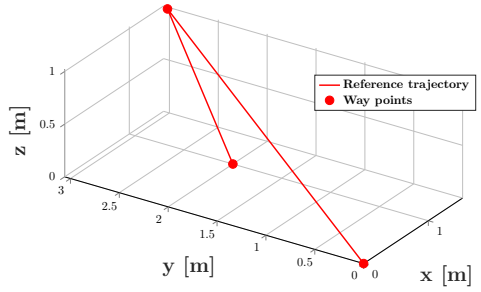

Fig. 3: Reference trajectory passing through three way points.

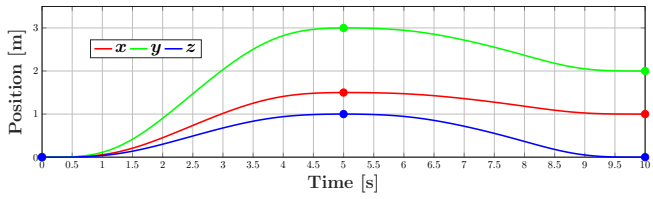

Fig. 4: Position references x, y, z passing through three way points.

From Fig. 3, one can misjudge that the trajectory is as simple as providing the step references passing through three way points but actually, each position components is described by the smooth B-spline curve as illustrated in Fig. 4. The resulted trajectory given in Fig. 3 proves the effectiveness of the optimization process which minimized the length of the trajectory.

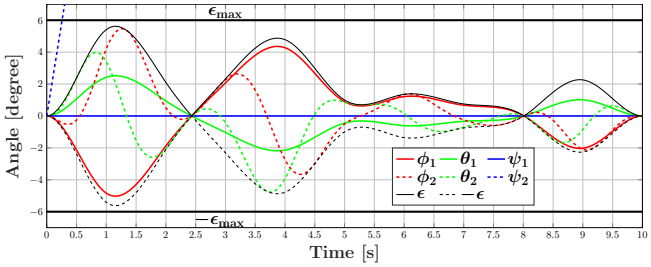

Fig. 5: The angle references under different scenarios, the angle ϵ and the angle boundary ϵ_{max}.

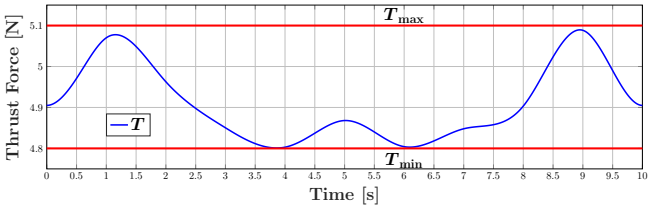

Fig. 6: Thrust reference and its boundary T_{min}, T_{max}.

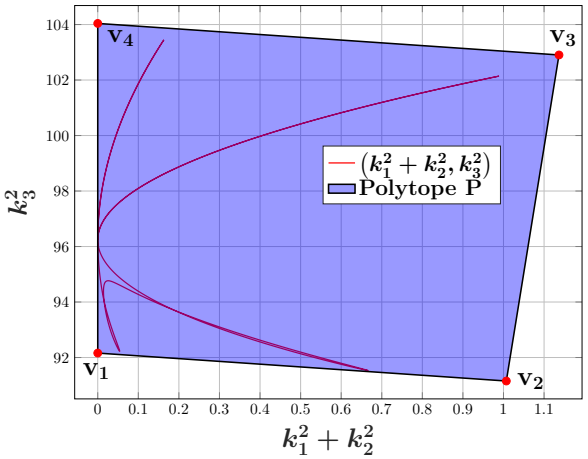

Fig. 7: Reference trajectory $(k_1^2 + k_2^2, k_3^2)$ (10) within the polytope P.

Hereinafter, we prove in Fig. 7 Corollary 1 which shows that the reference trajectory of $(k_1^2 + k_2^2, k_3^2)$ as given in (10) (plotted in solid red line) lies inside the polytope P described in (19). Satisfying Corollary 1 indicates that the references of the thrust T and of the roll and pitch angles under both scenarios satisfy their constraints (18), (11). This assertion is validated by Fig. 5–6. In Fig. 5, the references of the roll, pitch angles under both scenarios stay within the range $[-\epsilon, \epsilon]$ as given in (11). Also, the angle ϵ given in (13) does not exceed the limit, ϵ_{max} as stated in Proposition 2. Next, in Fig. 6, we show that the thrust reference T plotted in solid blue line lies in the range $[T_{min}, T_{max}]$ plotted by two solid red lines.

Moreover, Fig. 8a and 8b give the angular velocities Ω_x and Ω_y, respectively, where the references under Scenario 1, Ω_{x1}, Ω_{y1} are plotted in solid red lines, the results under Scenario 2, Ω_{x2}, Ω_{y2} in dashed green line. Under both

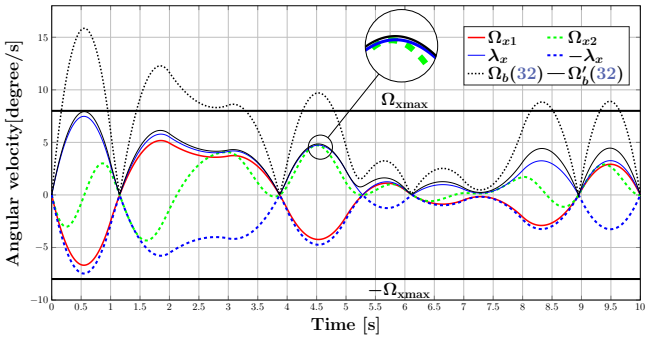

(a) Angular velocity about the ${}^{B}\boldsymbol{x}$ axis, Ω_x.

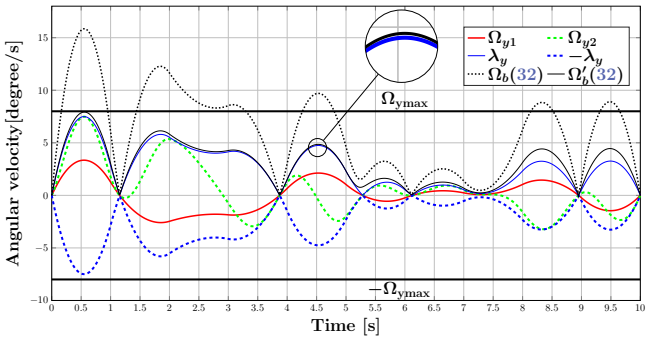

(b) Angular velocity about the ${}^{B}\boldsymbol{y}$ axis, Ω_y.

Fig. 8: References of the angular velocities Ω_x, Ω_y under two scenarios and comparison with [5] and [6].

scenarios, the references of the angular velocities lie inside $[-\lambda_x(t), \lambda_x(t)]$ and $[-\lambda_y(t), \lambda_y(t)]$ plotted in solid blue lines and dashed blue line, as detailed in (29), Section III-B. The boundary functions $\lambda_x(t)$ and $\lambda_y(t)$ do not exceed the limits Ω_{xmax} and Ω_{ymax} plotted in solid black lines which actually validate the imposed constraints on angular velocities (23), (24). Fig. 8a and 8b show that (at least for the particular choice of accelerations and jerks used here), the boundaries λ_x, λ_y from (30), (31) are tighter than Ω_b (dashed black line), Ω_b' (solid black line) from (32).

V. Conclusions

This paper addressed the constrained motion planning problem for the thrust-propelled systems by using differential flatness properties. Novel constraints on roll, pitch angles and the associated angular velocities are provided. The constraints, which can be applied for a vast class of underactuated aerial vehicles, are validated even with undefined yaw angle or uncontrolled yaw motion. These results were validated through proof of concept examples, illustrations and simulation results. Future work will analyze the robustness properties of the proposed constraints in the presence of disturbances and fault events.

References

[1] A. Roza, M. Maggiore, and L. Scardovi, "A class of rendezvous controllers for underactuated thrust-propelled rigid bodies," in *Proceeding of the 53rd Conference on Decision and Control (CDC)*. IEEE, 2014, pp. 1649–1654.

[2] B. Herissé, T. Hamel, R. Mahony, and F.-X. Russotto, "Landing a vtol unmanned aerial vehicle on a moving platform using optical flow," *IEEE Transactions on robotics*, vol. 28, no. 1, pp. 77–89, 2012.

[3] N. T. Nguyen, I. Prodan, F. Stoican, and L. Lefevre, "Reliable nonlinear control for quadcopter trajectory tracking through differential flatness," *IFAC-PapersOnLine*, vol. 50, no. 1, pp. 6971 – 6976, 2017.

[4] H. Lu, C. Liu, L. Guo, and W.-H. Chen, "Constrained anti-disturbance control for a quadrotor based on differential flatness," *International Journal of Systems Science*, vol. 48, no. 6, pp. 1182–1193, 2017.

[5] M. Hehn and R. D'Andrea, "Quadrocopter trajectory generation and control," *IFAC Proceedings Volumes*, vol. 44, no. 1, pp. 1485–1491, 2011.

[6] M. Hehn and R. DAndrea, "Real-time trajectory generation for quadrocopters," *IEEE Transactions on Robotics*, vol. 31, no. 4, pp. 877–892, 2015.

[7] T. Engelhardt, T. Konrad, B. Schäfer, and D. Abel, "Flatness-based control for a quadrotor camera helicopter using model predictive control trajectory generation," in *Proceedings of the 24th Mediterranean Conference on Control and Automation (MED'16)*. IEEE, 2016, pp. 852–859.

[8] F. Stoican, I. Prodan, D. Popescu, and L. Ichim, "Constrained trajectory generation for uav systems using a b-spline parametrization," in *Proceedings of the 25th Mediterranean Conference on Control and Automation (MED'17)*. IEEE, 2017, pp. 613–618.

[9] M. Fliess, J. Lévine, P. Martin, and P. Rouchon, "Flatness and defect of non-linear systems: introductory theory and examples," *International journal of control*, vol. 61, no. 6, pp. 1327–1361, 1995.

[10] I. D. Cowling, O. A. Yakimenko, J. F. Whidborne, and A. K. Cooke, "A prototype of an autonomous controller for a quadrotor uav," in *European Control Conference (ECC)*. IEEE, 2007, pp. 4001–4008.

[11] K. Bipin, V. Duggal, and K. M. Krishna, "Autonomous navigation of generic quadrocopter with minimum time trajectory planning and control," in *IEEE International Conference on Vehicular Electronics and Safety (ICVES)*. IEEE, 2014, pp. 66–71.

[12] N. T. Nguyen, I. Prodan, and L. Lefevre, "Multi-layer optimization-based control design for quadcopter trajectory tracking," in *Proceedings of the 25th Mediterranean Conference on Control and Automation (MED'17)*. IEEE, July 2017, pp. 601–606.

[13] I. S. Gradshteyn and I. M. Ryzhik, *Table of integrals, series, and products*. Academic press, 2014.

[14] G. M. Ziegler, *Lectures on polytopes*. Springer Science & Business Media, 2012, vol. 152.

[15] F. Stoican, I. Prodan, and D. Popescu, "Flat trajectory generation for way-points relaxations and obstacle avoidance," in *Proceedings of the 23th Mediterranean Conference on Control and Automation (MED'15)*. IEEE, 2015, pp. 695–700.

[16] J. Löfberg, "Yalmip : A toolbox for modeling and optimization in MATLAB," in *Proceedings of the CACSD Conference*, Taipei, Taiwan, 2004. [Online]. Available: http://users.isy.liu.se/johanl/yalmip

Appendix

A. The proof of the expressions of the angular velocities Ω_x and Ω_y in equation (28)

By applying some trigonometric manipulations to (7a), (7b), we have the following relations:

$$\mathrm{c}\,\phi\,\mathrm{s}\,\theta = \mathrm{c}\,\psi\,\mathrm{s}\,\phi_{\pi/2} - \mathrm{s}\,\psi\,\mathrm{s}\,\phi_0, \tag{33}$$

$$\mathrm{t}\,\phi = \mathrm{c}\,\theta\left(\mathrm{s}\,\psi\,\mathrm{t}\,\theta_0 - \mathrm{c}\,\psi\,\mathrm{t}\,\theta_{\pi/2}\right). \tag{34}$$

By introducing (33) into $\dot{\phi}$ derived from (7a) and (34) into $\dot{\theta}$ derived from (7b) and further expressing the results in terms of the notations in (22), the derivatives of the roll and pitch angles are given as:

$$\dot{\phi} = \frac{\mathrm{s}\,\psi\,\mathrm{c}\,\phi_{\pi/2}\dot{\phi}_{\pi/2} + \mathrm{c}\,\psi\,\mathrm{c}\,\phi_0\dot{\phi}_0}{\mathrm{c}\,\phi} + \dot{\psi}\,\mathrm{s}\,\theta, \tag{35}$$

$$\dot{\theta} = \mathrm{c}^2\,\theta\left(\frac{\mathrm{c}\,\psi\dot{\theta}_0}{\mathrm{c}^2\,\theta_0} + \frac{\mathrm{s}\,\psi\dot{\theta}_{\pi/2}}{\mathrm{c}^2\,\theta_{\pi/2}}\right) - \mathrm{t}\,\phi\,\mathrm{c}\,\theta\dot{\psi}. \tag{36}$$

Introducing (35) and (36) into (2) leads to:

$$\Omega_x = \frac{\mathrm{s}\,\psi\,\mathrm{c}\,\phi_{\pi/2}\dot{\phi}_{\pi/2} + \mathrm{c}\,\psi\,\mathrm{c}\,\phi_0\dot{\phi}_0}{\mathrm{c}\,\phi}, \tag{37}$$

$$\Omega_y = \mathrm{c}\,\phi\,\mathrm{c}^2\,\theta\left(\frac{\mathrm{c}\,\psi\dot{\theta}_0}{\mathrm{c}^2\,\theta_0} + \frac{\mathrm{s}\,\psi\dot{\theta}_{\pi/2}}{\mathrm{c}^2\,\theta_{\pi/2}}\right) \tag{38}$$

Equations (28) can be easily derived from (37), (38) by employing the flat representation of the yaw angle (7c), hence, completing the proof.